analytical chemistry

Letter

Cite This: Anal. Chem. XXXX, XXX, XXX−XXX

pubs.acs.org/ac

Desorption Electrospray Ionization Coupled with Ultraviolet Photodissociation for Characterization of Phospholipid Isomers in Tissue Sections

Dustin R. Klein, Clara L. Feider,[‡] Kyana Y. Garza,[‡] John Q. Lin, Livia S. Eberlin, and Jennifer S. Brodbelt*

Department of Chemistry, The University of Texas at Austin, Austin, Texas 78712, United States

Supporting Information

ABSTRACT: Desorption electrospray ionization (DESI) mass spectrometry imaging has become a powerful strategy for analysis of tissue sections, enabling differentiation of normal and diseased tissue based on changes in the lipid profiles. The most common DESI workflow involves collection of MS1 spectra as the DESI spray is rastered over a tissue section. Relying on MS1 spectra inherently limits the ability to differentiate isobaric and isomeric species or evaluate variations in the relative abundances of key isomeric lipids, such as double-bond positional isomers which may distinguish normal and diseased tissues. Here, 193 nm ultraviolet photodissociation (UVPD), a technique capable of differentiating double-bond positional isomers, is coupled with DESI to map differences in the double-bond isomer composition in tissue sections in a fast, high throughput manner compatible with imaging applications.

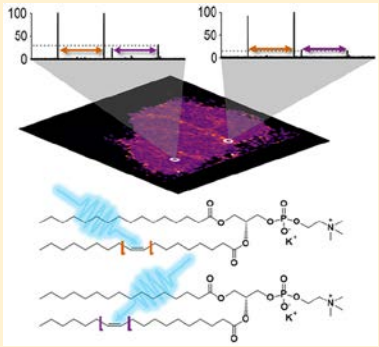

Mass spectrometry imaging (MSI) has emerged as a formidable tool to obtain spatially resolved chemical profiles from tissue sections, thus enhancing the diagnosis and prognosis of diseases like cancer.[1−4] The most widely used ionization techniques for MSI include matrix assisted laser desorption ionization (MALDI)[5,6] and desorption electrospray ionization (DESI).[7−9] MSI experiments are most commonly performed by collecting MS1 spectra as the ionization source is rastered over the tissue section with ion intensities subsequently plotted in two dimensions. Direct sampling of tissue produces complex mass spectra with isobaric species often overlapping or interfering with the analytes of interest. Implementation of MSI on high performance mass spectrometers has alleviated the problem of isobaric interferences and exposed the complexity of biomolecular profiles within tissue sections.[10−13] While high mass resolution and accuracy measurements facilitate analysis of congested spectra, collection of MS1 data provides little structural information on the detected species. Consequently, isomeric species remain indistinguishable by MS1 alone; however, structural characterization via tandem mass spectrometry (MS/MS) provides one approach for deciphering isomers and increasing analyte specificity.[14,15]

Collisionally activated dissociation (CAD) is the most common MS/MS method used for structural characterization, particularly for lipids.[16] However, a number of subtle features with significant biological implications, including double-bond position, acyl chain *sn*-position, and double-bond stereochemistry, are frequently not confirmed by CAD.[17] Differences in the spatial distribution of isomers arising from these features therefore go unresolved. In particular, double-bond positions have been shown to greatly influence lipid membrane thickness and ordering[18] and play a substantial role in protein−lipid binding.[19] In addition, changes in the relative abundances of double-bond positional isomers have shown promise for differentiation of normal and diseased tissues.[20] Advances in ion mobility spectrometry have enabled fast separation of lipid isomers in the gas phase,[21,22] and tandem mass spectrometry is crucial for identification of the separated lipids. In-spray Paternò-Büchi reactions with subsequent collisional activation of reaction products have demonstrated success as a means to determine double-bond positions.[23,24] Alternatively, novel ion activation methods are another strategy to elucidate double-bond positions. These include high-energy CID,[25,26] radical-directed dissociation,[27,28] electron-induced dissociation,[29,30] electron impact excitation of ions from organics,[31,32] ozone-induced dissociation (OzID),[33−37] and metastable atom-activated dissociation.[38,39] Ultraviolet photodissociation (UVPD) at 193 nm has also proven to be a compelling ion activation method for lipid characterization.[40−43] For glycerophospholipids and sphingolipids, UVPD generates sets of ions that are diagnostic for determining double-bond position.[41−43]

Of the aforementioned methods, only a few have been used for profiling double-bond positional isomers *in situ*.[24,25,34,37] High-energy CID performed on a MALDI-TOF instrument allowed the detailed structural characterization of glycerophos-

Received: July 5, 2018
Accepted: August 6, 2018
Published: August 6, 2018

DOI: 10.1021/acs.analchem.8b03026
Anal. Chem. XXXX, XXX, XXX−XXX

pholipids in mouse brain tissue.[25] OzID has been integrated with a DESI platform for the detection of lipid *sn*-positional isomers in tissue sections[34] and more recently to a MALDI-Orbitrap for MSI of lipid isomer spatial distribution.[37] Paternò-Büchi reactions have been coupled with a liquid microjunction surface sampling probe system for profiling and quantitation of double-bond positional isomers *in situ*.[24] In the present study, DESI is performed on an Orbitrap mass spectrometer equipped with 193 nm UVPD to map spatial distributions of double-bond isomers *in situ*. Our findings reveal that there are changes in the relative abundances of lipid isomers localized to specific tissue features, demonstrating for the first time that

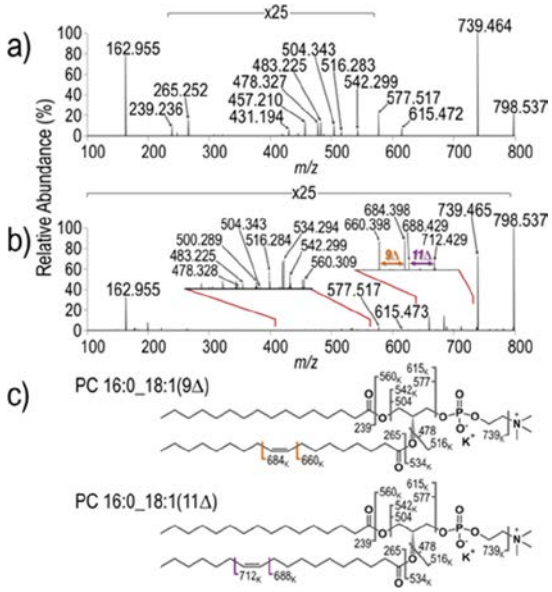

Figure 1. (a) HCD (NCE 30) and (b) UVPD (20 pulses, 6 mJ) mass spectra of the ion of m/z 798 obtained from DESI profiling of a mouse brain tissue section with (c) corresponding fragment ion maps for detected isomers [PC 16:0_18:1(9Δ), PC 16:0_18:1(11Δ)]. The subscript "K" in the labels of the fragment ion maps indicate ions that the potassium adduct is retained.

ambient MSI integrated with UVPD-MS allows direct characterization of double-bond isomers in tissue.

DESI was implemented on an Orbitrap Fusion Lumos mass spectrometer (Figure S1). Higher-energy collisional dissociation (HCD) and UVPD mass spectra for the prominent ion of m/z 798 with corresponding fragment ion maps are shown in Figure 1. Product and neutral loss ions in the HCD spectrum confirm the identity of this species as potassium-adducted phosphatidylcholine PC 16:0_18:1. The UVPD mass spectrum provides greater structural detail, confirming the occurrence of at least two double-bond positional isomers, namely, PC 16:0_18:1(9Δ) and PC 16:0_18:1(11Δ), through sets of diagnostic ions spaced apart by 24 Da. These pairs of fragment ions separated by 24 Da are signatures generated uniquely by UVPD and are highly characteristic of double-bond position, as reported previously.[41−43] HCD and UVPD mass spectra for the sodium-adducted and protonated species of PC 16:0_18:1 provide comparable information to the potassium-adducted ion, indicating that acyl chain composition and double-bond information can be obtained regardless of adduction status (Figures S2−S4). Despite the magnification of the key

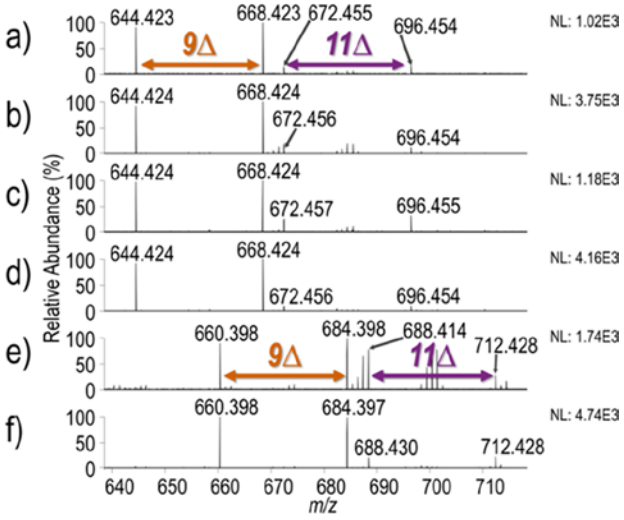

Figure 2. Expansions of UVPD (20 pulses, 6 mJ) mass spectra from DESI profiling of (a) endometrial tissue (m/z 782), (b) kidney tissue (m/z 782), (c) lymph node tissue (m/z 782), (d) ovarian tissue (m/z 782), (e) pancreas tissue (m/z 798), and (f) brain tissue (m/z 798), showcasing the key diagnostic ions that differentiate two isomeric lipids [PC 16:0_18:1(9Δ), PC 16:0_18:1(11Δ)]. The full m/z range HCD and UVPD mass spectra are shown in Figures S8 and S9.

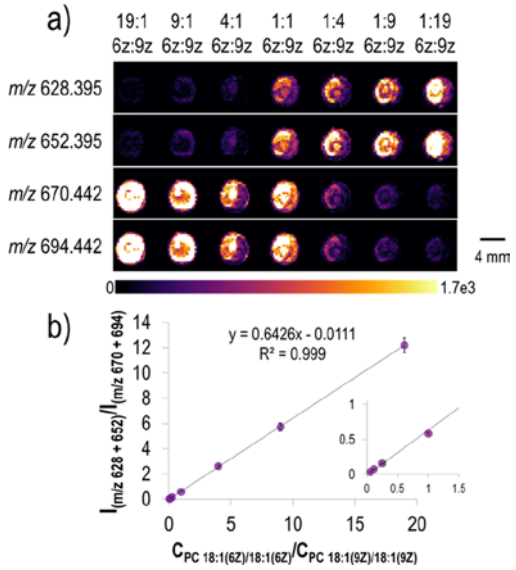

Figure 3. (a) DESI-UVPD ion images of two isomeric phospholipid standards, PC 18:1(6Z)/18:1(6Z) and PC 18:1(9Z)/18:1(9Z), in varying concentration ratios. Each pair of product ions diagnostic for the double-bond position are tracked. (b) Plot of concentration ratio of PC 18:1(6Z)/18:1(6Z) to PC 18:1(9Z)/18:1(9Z) ($C_{PC\ 18:1(6Z)/18:1(6Z)}/C_{PC\ 18:1(9Z)/18:1(9Z)}$) versus the ratio of the summed intensities of the diagnostic ions ($I_{(m/z\ 628+652)}/I_{(m/z\ 670+694)}$).

fragment ion region in some of the MS/MS spectra, S/N ratios of >100 were routinely obtained owing to the high sensitivity of the Orbitrap analyzer. HCD and UVPD mass spectra were also collected for other high abundance ions of m/z 826 and m/z 820 in the lipid profile spectrum (Figures S5 and S6). The UVPD mass spectra for these other lipids reveal that they are each composed of at least two double-bond positional isomers, PC 18:0_18:1(9Δ) and PC

DOI: 10.1021/acs.analchem.8b03026
Anal. Chem. XXXX, XXX, XXX−XXX

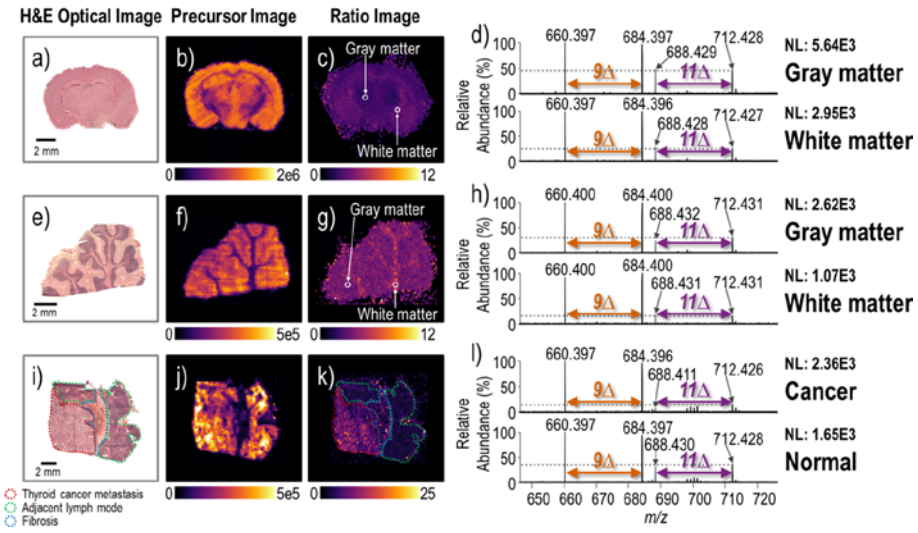

Figure 4. Optical images of the H&E stained (a) mouse brain tissue section, (e) human brain tissue section, and (i) lymph node tissue section with thyroid cancer metastasis. (b) DESI-MS ion image of m/z 798, (c) DESI-UVPD ratio image of the ratio of the summed intensities of the UVPD double-bond diagnostic ions ($I_{m/z\ 660+684}$)/($I_{m/z\ 688+712}$), (d) expanded region of UVPD mass spectra of the white and gray matter, (f) DESI-MS ion image of m/z 798, (g) DESI ratio image of the ratio of the summed intensities of the UVPD double-bond diagnostic ions ($I_{m/z\ 660+684}$)/($I_{m/z\ 688+712}$), (h) expanded region of UVPD mass spectra of the white and gray matter, (j) DESI-MS ion image of m/z 798, (k) DESI ratio image of the intensity m/z 684 divided by the intensity m/z 712, and (l) expanded regions of UVPD mass spectra of cancerous and normal parts of tissue. Representative spectra were taken from areas of tissue marked with a white arrow. DESI-UVPD ion images of each double-bond diagnostic ions ($I_{m/z\ 660}$, $I_{m/z\ 684}$, $I_{m/z\ 688}$, and $I_{m/z\ 712}$), DESI-UVPD ratio images, and corresponding spectra are in Figures S14−S19.

18:0_18:1(11Δ) for m/z 826 and PC 16:0_20:4-(5Δ,8Δ,11Δ,14Δ) for m/z 820, on the basis of the presence of paired fragment ions separated by 24 Da. This evidence confirms that UVPD is capable of localizing the positions of multiple double bonds within a single acyl chain for lipids desorbed from tissue.

DESI profiling experiments were performed on a number of human tissue types, including endometrial, kidney, lymph node, ovarian, pancreas, and brain (Figures 2 and S7−S9). Figure 2 shows expanded regions of the UVPD mass spectra for sodium-adducted and potassium-adducted ions of m/z 782 or m/z 798, respectively, collected for each tissue type, focusing on the diagnostic fragment ions used to identify double-bond isomers. While the PC 16:0_18:1(9Δ) isomer is consistently more dominant across the tissue types based on the greater abundance of the m/z 644/668 or m/z 660/684 ion pair (corresponding to the 9Δ isomer) relative to the m/z 672/696 or m/z 688/712 ion pair (11Δ isomer), respectively, there is a notable change in the relative abundances of PC 16:0_18:1(9Δ) and PC 16:0_18:1(11Δ) across all five tissue types. In some of the mass spectra, most notably Figure 2e, additional product ions are present, corresponding to fragment ions from lipid species that are isobaric to the lipid of interest. The high resolving power and mass accuracy of the Orbitrap mass analyzer allows these product ions from isobaric species to be differentiated from specific diagnostic ions. Integration of the UVPD method on an imaging mass spectrometer also equipped with ion mobility separation capabilities is an intriguing idea that may enable acquisition of MS/MS spectra free from extraneous ion peaks.

The profiling mode experiments described above confirmed the successful differentiation of isomeric lipids by UVPD, thus motivating the exploration of UVPD for tissue imaging experiments. To determine the ability of UVPD to discern spatially resolved differences in the relative abundances of phospholipid isomers during DESI-MSI, a set of phospholipid isomer standards, PC 18:1(6Z)/18:1(6Z) and PC 18:1(9Z)/18:1(9Z), in varying concentration ratios and with a summed concentration of 10 μM, were spotted onto a glass slide and imaged (Figure 3). UVPD mass spectra of m/z 808, corresponding to a sodium-adducted ion, shown in Figure S10, provide structural confirmation of the isomers, with UVPD mass spectra containing diagnostic sets of ions of m/z 628 and m/z 652 for PC 18:1(6Z)/18:1(6Z) and m/z 670 and m/z 694 for PC 18:1(9Z)/18:1(9Z). Changes in ion intensities in the DESI-UVPD images of each diagnostic ion correlate with variations in the lipid concentration ratios (Figures 3a and S11). Excellent agreement (R^2 = 0.999) between the concentration ratio of PC 18:1(6Z)/18:1(6Z) to PC 18:1(9Z)/18:1(9Z) ($C_{\mathrm{PC\ 18:1(6Z)/18:1(6Z)}}$/$C_{\mathrm{PC\ 18:1(9Z)/18:1(9Z)}}$) and the ratio of summed diagnostic ion intensities ($I_{m/z\ 628+652}$)/$I_{m/z\ 670+694}$) was achieved (Figure 3b). The lowest concentration detectable based on the UVPD-MS method was estimated to be ∼500 nM. These results confirm that the developed DESI-UVPD-MSI method can successfully detect changes in the relative abundances of phospholipid isomers in two dimensions, indicating that differences detected in tissue should directly result from changes in isomer concentrations.

DESI-UVPD-MSI experiments were performed in triplicate for coronal mouse brain tissue sections (Figures 4a−d and S12−S14). H&E optical images for all tissues were collected after collection of DESI data. The MS1 DESI ion image (Figure 4b) reveals a lower abundance of the lipid ion of m/z 798 (corresponding to PC 16:0_18:1) in the white matter compared to the gray matter. DESI-UVPD ion images for each of the diagnostic ions previously detected during DESI-UVPD profiling experiments are shown for each replicate ($I_{m/z\ 660}$, $I_{m/z\ 684}$, $I_{m/z\ 688}$, and $I_{m/z\ 712}$), along with images of the summed intensities of the diagnostic ions ($I_{m/z\ 660+684}$, $I_{m/z\ 688+712}$).

DOI: 10.1021/acs.analchem.8b03026
Anal. Chem. XXXX, XXX, XXX−XXX

Images of the ratio of the summed intensities of the diagnostic ions ($I_{m/z\ 660+684}/I_{m/z\ 688+712}$) demonstrate that there are, in fact, notable changes in the relative abundances of PC 16:0_18:1(9Δ) and PC 16:0_18:1(11Δ) throughout the tissue corresponding to areas of gray matter and white matter. Key expanded regions of the representative UVPD mass spectra of gray and white matter are shown in Figure 4d. While the overall abundance of m/z 798 appears to decrease in the white matter based on DESI-MSI data, the ratio of PC 16:0_18:1(9Δ) to PC 16:0_18:1(11Δ) increases in the white matter relative to the gray matter. Our observations of changes in the relative abundances of isomers between white matter and gray matter are consistent with results recently obtained by Paine et al.[37] A similar observation is drawn for human brain tissue (Figures 4e–h and S15) with branches of white matter in the human brain section observed in both the optical and DESI images.

DESI-UVPD-MSI also offers the unique opportunity to investigate differences in the abundances of lipid isomers between normal and cancerous regions of tissue sections. DESI-UVPD-MSI was performed on a section of human lymph node tissue containing thyroid cancer metastasis based on monitoring the ion of m/z 798 (Figure 4i–l).[44] The presence of both PC 16:0_18:1(9Δ) and PC 16:0_18:1(11Δ) was confirmed by UVPD-MS based on the paired fragment ions (Figures S17 and S18). One selected ion from each pair of diagnostic ions was used to create a ratio image that revealed a distinctive change in the relative abundance of the two lipid isomers between normal and diseased tissue (Figure S18). Although there appears to be a change in the relative abundances of the two isomers between the normal and cancerous portions of tissue, a larger sample set is required to assess if DESI-UVPD-MSI is capable of differentiating normal and cancerous tissue.

This study represents the first coupling of ambient MSI with an ion activation technique capable of determining double-bond positions in phospholipid acyl chains. DESI-UVPD not only differentiates phospholipid isomers but also unveils spatial changes in their relative abundances that are otherwise undetected during DESI-MSI experiments. The short activation period of UVPD enables fast acquisition of diagnostic MS/MS information. Considering the informative spectra generated by UVPD, application of this method to other types of lipids offers the potential to provide insights into the processes that result in altered lipid metabolism.

■ ASSOCIATED CONTENT

Supporting Information

The Supporting Information is available free of charge on the ACS Publications website at DOI: 10.1021/acs.analchem.8b03026.

Experimental methods; Figure S1, image of experimental setup and MS1 spectrum; Figures S2–S6, HCD and UVPD spectra and fragment ion maps of m/z 760, 782, 798, 826, and 820; Figures S7–S9, MS1, HCD, and UVPD DESI profiling spectra; Figure S10, HCD and UVPD spectra of PC 18:1(6Z)/18:1(6Z) and 18:1(9Z)/18:1(9Z); Figure S11, UVPD spectra of PC 18:1(6Z)/18:1(6Z) and 18:1(9Z)/18:1(9Z) in varying concentration ratios; Figures S12–S16, DESI-UVPD ion images; Figures S17 and S18, HCD and UVPD DESI profiling spectra from lymph node tissue section with thyroid cancer metastasis (PDF)

■ AUTHOR INFORMATION

Corresponding Author

*E-mail: jbrodbelt@cm.utexas.edu.

ORCID

Livia S. Eberlin: 0000-0002-3885-3215

Jennifer S. Brodbelt: 0000-0003-3207-0217

Author Contributions

‡C.L.F. and K.Y.G. contributed equally to this work.

Notes

The authors declare no competing financial interest.

■ ACKNOWLEDGMENTS

Support from the NIH (R00CA190783 to L.S.E. and R01 GM103655 to J.S.B.) and the Welch Foundation (F-1895 to L.S.E. and F-1155 to J.S.B.) is gratefully acknowledged. We thank the Department of Physics machine shop for fabrication of the ion transfer tube. Funding from the UT System for support of the UT System Proteomics Core Facility Network is gratefully acknowledged. We thank the NCI Cooperative Human Tissue Network (CHTN) for proving human tissue samples and Dr. Wendong Yu (Baylor College of Medicine) for histopathologic evaluation.

■ REFERENCES

(1) Amstalden van Hove, E. R.; Smith, D. F.; Heeren, R. M. A. *J. Chromatogr. A* **2010**, *1217*, 3946–3954.

(2) Gode, D.; Volmer, D. A. *Analyst* **2013**, *138*, 1289–1315.

(3) Vaysse, P.; Heeren, R. M. A.; Porta, T.; Balluff, B. *Analyst* **2017**, *142*, 2690–2712.

(4) Sans, M.; Gharpure, K.; Tibshirani, R.; Zhang, J.; Liang, L.; Liu, J.; Young, J. H.; Dood, R. L.; Sood, A. K.; Eberlin, L. S. *Cancer Res.* **2017**, *77*, 2903–2913.

(5) Norris, J. L.; Caprioli, R. M. *Chem. Rev.* **2013**, *113*, 2309–2342.

(6) Gessel, M. M.; Norris, J. L.; Caprioli, R. M. *J. Proteomics* **2014**, *107*, 71–82.

(7) Wiseman, J. M.; Ifa, D. R.; Song, Q.; Cooks, R. G. *Angew. Chem., Int. Ed.* **2006**, *45*, 7188–7192.

(8) Ifa, D. R.; Wu, C.; Ouyang, Z.; Cooks, R. G. *Analyst* **2010**, *135*, 669–681.

(9) Eberlin, L. S.; Ferreira, C. R.; Dill, A. L.; Ifa, D. R.; Cooks, R. G. *Biochim. Biophys. Acta, Mol. Cell Biol. Lipids* **2011**, *1811*, 946–960.

(10) Bereman, M. S.; Nyadong, L.; Fernandez, F. M.; Muddiman, D. C. *Rapid Commun. Mass Spectrom.* **2006**, *20*, 3409–3411.

(11) Pól, J.; Vidová, V.; Kruppa, G.; Kobliha, V.; Novák, P.; Lemr, K.; Kotiaho, T.; Kostiainen, R.; Havlíček, V.; Volný, M. *Anal. Chem.* **2009**, *81*, 8479–8487.

(12) Manicke, N. E.; Dill, A. L.; Ifa, D. R.; Cooks, R. G. *J. Mass Spectrom.* **2010**, *45*, 223–226.

(13) Römpp, A.; Spengler, B. *Histochem. Cell Biol.* **2013**, *139*, 759–783.

(14) Lietz, C. B.; Gemperline, E.; Li, L. *Adv. Drug Delivery Rev.* **2013**, *65*, 1074–1085.

(15) Prideaux, B.; Dartois, V.; Staab, D.; Weiner, D. M.; Goh, A.; Via, L. E.; Barry, C. E.; Stoeckli, M. *Anal. Chem.* **2011**, *83*, 2112–2118.

(16) Pulfer, M.; Murphy, R. C. *Mass Spectrom. Rev.* **2003**, *22*, 332–364.

(17) Harayama, T.; Riezman, H. *Nat. Rev. Mol. Cell Biol.* **2018**, *19*, 281–296.

(18) Martinez-Seara, H.; Róg, T.; Pasenkiewicz-Gierula, M.; Vattulainen, I.; Karttunen, M.; Reigada, R. *J. Phys. Chem. B* **2007**, *111*, 11162–11168.

DOI: 10.1021/acs.analchem.8b03026
Anal. Chem. XXXX, XXX, XXX–XXX

(19) Shinzawa-Itoh, K.; Aoyama, H.; Muramoto, K.; Terada, H.; Kurauchi, T.; Tadehara, Y.; Yamasaki, A.; Sugimura, T.; Kurono, S.; Tsujimoto, K.; Mizushima, T.; Yamashita, E.; Tsukihara, T.; Yoshikawa, S. *EMBO J.* **2007**, *26*, 1713−1725.
(20) Ma, X.; Chong, L.; Tian, R.; Shi, R.; Hu, T. Y.; Ouyang, Z.; Xia, Y. *Proc. Natl. Acad. Sci. U. S. A.* **2016**, *113*, 2573−2578.
(21) Groessl, M.; Graf, S.; Knochenmuss, R. *Analyst* **2015**, *140*, 6904−6911.
(22) Hancock, S. E.; Poad, B. L. J.; Batarseh, A.; Abbott, S. K.; Mitchell, T. W. *Anal. Biochem.* **2017**, *524*, 45−55.
(23) Ma, X.; Xia, Y. *Angew. Chem.* **2014**, *126*, 2630−2634.
(24) Tang, F.; Guo, C.; Ma, X.; Zhang, J.; Su, Y.; Tian, R.; Shi, R.; Xia, Y.; Wang, X.; Ouyang, Z. *Anal. Chem.* **2018**, *90*, 5612−5619.
(25) Shimma, S.; Kubo, A.; Satoh, T.; Toyoda, M. *PLoS One* **2012**, *7*, e37107.
(26) Toyoda, M. *Eur. J. Mass Spectrom.* **2010**, *16*, 397−406.
(27) Pham, H. T.; Ly, T.; Trevitt, A. J.; Mitchell, T. W.; Blanksby, S. J. *Anal. Chem.* **2012**, *84*, 7525−7532.
(28) Pham, H. T.; Trevitt, A. J.; Mitchell, T. W.; Blanksby, S. J. *Rapid Commun. Mass Spectrom.* **2013**, *27*, 805−815.
(29) Yoo, H. J.; Håkansson, K. *Anal. Chem.* **2010**, *82*, 6940−6946.
(30) Jones, J. W.; Thompson, C. J.; Carter, C. L.; Kane, M. A. *J. Mass Spectrom.* **2015**, *50*, 1327−1339.
(31) Campbell, J. L.; Baba, T. *Anal. Chem.* **2015**, *87*, 5837−5845.
(32) Baba, T.; Campbell, J. L.; Yves Le Blanc, J. C.; Baker, P. R. S. *J. Lipid Res.* **2016**, *57*, 858−867.
(33) Pham, H. T.; Maccarone, A. T.; Thomas, M. C.; Campbell, J. L.; Mitchell, T. W.; Blanksby, S. J. *Analyst* **2014**, *139*, 204−214.
(34) Kozlowski, R. L.; Mitchell, T. W.; Blanksby, S. J. *Sci. Rep.* **2015**, *5*, 9243.
(35) Poad, B. L. J.; Green, M. R.; Kirk, J. M.; Tomczyk, N.; Mitchell, T. W.; Blanksby, S. J. *Anal. Chem.* **2017**, *89*, 4223−4229.
(36) Poad, B. L. J.; Zheng, X.; Mitchell, T. W.; Smith, R. D.; Baker, E. S.; Blanksby, S. J. *Anal. Chem.* **2018**, *90*, 1292−1300.
(37) Paine, M. R. L.; Poad, B. L. J.; Eijkel, G. B.; Marshall, D. L.; Blanksby, S. J.; Heeren, R. M. A.; Ellis, S. R. *Angew. Chem.* **2018**, *130*, 10690.
(38) Deimler, R. E.; Sander, M.; Jackson, G. P. *Int. J. Mass Spectrom.* **2015**, *390*, 178−186.
(39) Li, P.; Hoffmann, W. D.; Jackson, G. P. *Int. J. Mass Spectrom.* **2016**, *403*, 1−7.
(40) Brodbelt, J. S. *Chem. Soc. Rev.* **2014**, *43*, 2757−2783.
(41) Klein, D. R.; Brodbelt, J. S. *Anal. Chem.* **2017**, *89*, 1516−1522.
(42) Williams, P. E.; Klein, D. R.; Greer, S. M.; Brodbelt, J. S. *J. Am. Chem. Soc.* **2017**, *139*, 15681−15690.
(43) Ryan, E.; Nguyen, C. Q. N.; Shiea, C.; Reid, G. E. *J. Am. Soc. Mass Spectrom.* **2017**, *28*, 1406−1419.
(44) Zhang, J.; Feider, C. L.; Nagi, C.; Yu, W.; Carter, S. A.; Suliburk, J.; Cao, H. S. T.; Eberlin, L. S. *J. Am. Soc. Mass Spectrom.* **2017**, *28*, 1166−1174.

DOI: 10.1021/acs.analchem.8b03026
Anal. Chem. XXXX, XXX, XXX−XXX